Atmospheric Research 256 (2021) 105585

Contents lists available at ScienceDirect

Atmospheric Research

journal homepage: www.elsevier.com/locate/atmosres

Significant impacts of anthropogenic activities on monoterpene and oleic acid-derived particulate organic nitrates in the North China Plain

Jun Zhang [a], Xinfeng Wang [a,*], Rui Li [a,b], Shuwei Dong [a], Jing Chen [a], Yingnan Zhang [a], Penggang Zheng [a], Min Li [a], Tianshu Chen [a], Yuhong Liu [a], Likun Xue [a], Xuehua Zhou [a], Lin Du [a], Qingzhu Zhang [a], Wenxing Wang [a,*]

[a] Environment Research Institute, Shandong University, Qingdao 266237, China
[b] State Key Laboratory of Organic Geochemistry, Guangzhou Institute of Geochemistry, Chinese Academy of Sciences, Guangzhou 510640, China

ARTICLE INFO

Keywords:
Particulate organic nitrate
Secondary formation
Biomass burning
Coal combustion
North China Plain

ABSTRACT

Particulate organic nitrates (PONs) are among the major components of organic aerosols and affect the reactive nitrogen budget and ozone formation on regional scale. Previous laboratory and field studies have shown some preliminary evidence for the effects of anthropogenic activities on the formation of PONs. In this study, the concentrations of six kinds of PONs in rural and urban areas in the North China Plain were determined, and the seasonal and diurnal difference and effects of anthropogenic activities on their formation were investigated. The average total concentration of PONs was in the range of 113– 415 ng m^{-3}, contributing 0.7% –2.8% to organic matter during the observation periods. Distinct seasonal variation was observed, with higher concentrations appearing in summer than in winter due to the large emissions of precursor BVOCs and intensive photochemical activities in the hot season. The concentration and formation of some specific PONs exhibited diurnal differences in summer, while the differences were small in other seasons. The observations showed that PONs in the North China Plain were significantly influenced by open biomass burning and coal combustion. The formation of PONs was enhanced by increased BVOCs released from biomass burning and consequently elevated levels of ozone. Industrial and residential coal combustion contributed to the increased concentrations of PONs by providing related reactants and interfaces and facilitating the formation rates of PONs.

1. Introduction

Particulate organic nitrates (PONs) are regarded as important components of organic aerosols (OA) and play significant roles in the regional reactive nitrogen recycling, ozone (O_3) production, and cloud formation. The contribution of PONs to organic aerosols was estimated 2–12% in southeastern United States in summer (Rollins et al., 2012; Xu et al., 2015). In addition, PONs are recognized as important temporary reservoir for nitrogen oxides (NO_x) and 52% of sequestered NO_x can be released again into the atmosphere (Horowitz et al., 2007; Zare et al., 2018). As the persistence of hydrophilic functional groups, PONs also tend to increase the hygroscopicity and thus serve as cloud condensation nuclei of aerosols (Novakov and Penner, 1993). Owing to the important effects of PONs on atmospheric chemistry and air quality, the chemical characterization and formation process have drawn close attention in both laboratory experiments and field observations.

Laboratory studies have revealed that organic nitrates can be formed by gas-phase reactions of biogenic volatile compounds (BVOCs) with atmospheric oxidants (OH radical, ozone, and NO_3 radical) in the presence of NO_x. The production of organic nitrates is mostly induced by OH radicals during the daytime, while NO_3 radicals are dominant during nighttime (Ng et al., 2017; Sobanski et al., 2017). Under the condition of low NO_x, RO_2 radicals formed from VOC oxidation mainly react with HO_2 to produce hydroperoxides. As the NO_x level increases, RO_2 radicals are more likely to react with NO to form organic nitrates (Hallquist et al., 2009; Zhao et al., 2018; Ziemann and Atkinson, 2012). Once the multifunctional organic nitrate is formed, it is ready to partition from the gas phase to the particle phase due to the low volatility (Ehn et al., 2014). The yield of organic nitrates and their contribution to OA usually increase with increasing NO_x, indicative of the promoting effect of anthropogenic emissions (Xu et al., 2020; Zhao et al., 2018). In addition, Han et al. (2016) observed that particle acidity had a positive effect on

* Corresponding authors.
E-mail addresses: xinfengwang@sdu.edu.cn (X. Wang), wxwang@sdu.edu.cn (W. Wang).

https://doi.org/10.1016/j.atmosres.2021.105585
Received 26 November 2020; Received in revised form 28 January 2021; Accepted 17 March 2021
Available online 19 March 2021

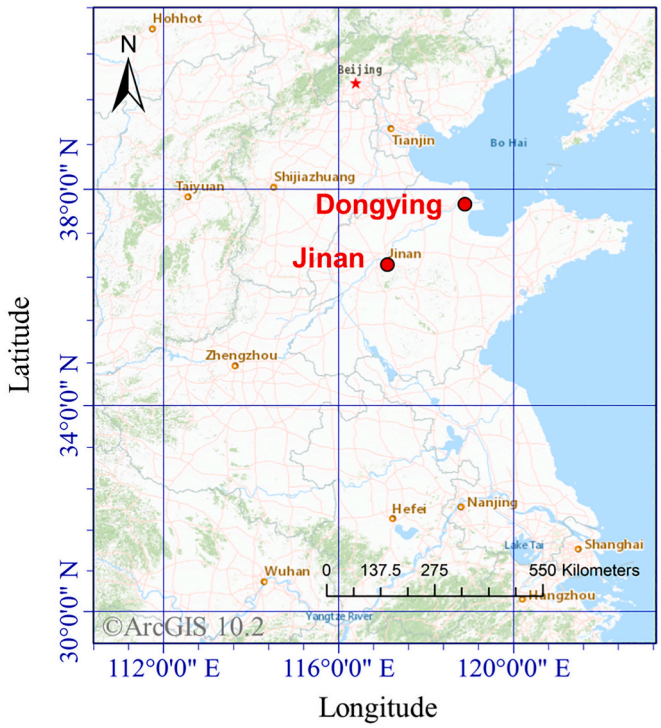

Fig. 1. Locations of the DY site and JN site deployed in this study.

the production of PONs under high-NO_x conditions, but the potential mechanism leading to the acid catalysis on the formation of PONs was unrevealed by the current knowledge. Besides that, the discrepancies in the PON yield and the ambient concentration between model prediction and field observation indicate that the current understanding of chemical reactions and formation processes of PONs is possibly incomplete (Pye et al., 2015).

Field observations have demonstrated that PONs are ubiquitous in ambient air and influenced by anthropogenic activities. Spatially extensive measurements in the United States and Europe show that high concentrations of PONs (with the maximum of 2.8 μg m^{-3}) were usually found in areas with large anthropogenic emissions, whereas low levels of PONs were often observed in remote regions (Kiendler-Scharr et al., 2016; Reyes-Villegas et al., 2018; Rollins et al., 2012; Xu et al., 2015). Fossil fuel burning such as vehicle exhausts and thermal power plant fumes was primarily responsible for the high concentrations of PONs in urban areas (Brown et al., 2012; Day et al., 2010; Fry et al., 2018). Fry et al. (2018) examined the nighttime aircraft transects of plumes from coal-fired power plants in the southeastern United States and provided evidence that the increase in organic nitrates was resulted from the rises in isoprene and NO_3 radical. Day et al. (2010) reported that the high levels of PONs were associated with the mixed modern fossil fuel combustion emissions, suggesting the enhancement of PON formation in polluted conditions. Taken together, field measurements in the United States and Europe suggest that PONs partly exist as a coupled anthropogenic–biogenic product that may be regionally significant. As in polluted atmosphere in the North China Plain where the emissions and abundances of anthropogenic and biogenic precursors are different from those in the US and Europe, the concentrations and main sources of PONs remain poorly understood. Based on the latest observations of PONs in China, a large disparity exists in the observed species and concentrations of PONs (Li et al., 2018; Shi et al., 2020; Wang et al., 2018b; Yu et al., 2019; Zhang et al., 2016). Zhang et al. (2016) observed the total concentration of particle phase organic nitrates was as high as 4.2 μg m^{-3} during the biomass burning period in Beijing, China, indicating that biomass burning is an important contributor to PONs. Moreover, anthropogenic VOCs (e.g. styrene) were considered as a kind of key precursors for PONs in Shenzhen, China (Yu et al., 2019). By far, there is a lack of comprehensive understanding on the impacts of anthropogenic activities on the formations of specific organic nitrates in polluted atmosphere environments in China, and more field measurements in different locations and seasons are required to perform a careful evaluation.

The North China Plain is densely populated and industrialized regions with intensive anthropogenic emissions. In the past decade, fine particulate matter ($PM_{2.5}$) and haze pollutions frequently occured here (Guo et al., 2014; Liu et al., 2020; Wang et al., 2014; Wen et al., 2018). Human activities such as open straw and crop burning after harvest and coal combustion for heating demand in winter have been recognized as the main sources of particulate matters and organic aerosols (de Oliveira Alves et al., 2014; Yu et al., 2013; Zong et al., 2018). In this study, six kinds of PONs were measured in rural and urban areas in the North China Plain. The seasonal and diurnal variations in concentration were investigated. The potential influences of open biomass burning and coal combustion on the enhancements of PONs were also discussed.

2. Experiments and methods

2.1. Site descriptions

The field measurement was carried out at a rural site in Dongying (DY) and an urban site in Jinan (JN) in the North China Plain (see Fig. 1). The DY site is located at the Yellow River Delta Ecology Research Station of Coastal Wetland (37°76′ N, 118°98′ E), in Dongying, Shandong Province. This sampling site is close to wide wetlands with rich biological resources. It is far from residential area and thus has few local anthropogenic emissions. The filter sampling and online measurements at the rural site of DY were conducted in both winter (15–23 January) and summer (4 June–9 July) of 2017. Detailed information of the DY site was given by Zhang et al. (2019).

The Jinan (JN) site is situated at the Atmospheric Environment Observatory Station in Shandong University (36°40′ N, 117°03′ E), in Jinan, Shandong Province. Jinan is a densely populated and industrialized city. There are heavy industries such as steel plants, cement plants, coal-fired power plants, and oil refinery plant, within 5–20 km to the northeast and southwest of the sampling site. The filter sampling in the urban site of JN was conducted from 20 October to 1 November 2017. More descriptions about the JN site can be found in Li et al. (2018).

2.2. Sampling and online measurements

$PM_{2.5}$ medium-volume (100 L min^{-1}) sampler (TH-150A, Wuhan Tianhong, China) was utilized to collect $PM_{2.5}$ samples. Particles with aerodynamic diameters of smaller than 2.5 μm were collected on quartz-fiber filters, which were pre-baked before utilization to remove organic matter that might absorb. The sampling were conducted during the daytime (8:00–19:30, local time, the same hereinafter) and nighttime (20:00–7:30) separately. After sampling, the filters were weighted to obtain the mass concentrations of particulate matter in the condition of constant relative humidity (RH, 50 ± 2%) and temperature (T, 20 ± 0.5 °C).

The real-time measurements of gaseous species and meteorological parameters at the DY site are introduced as follows. The trace gases measured included NO_2 (Teledyne Advanced Pollution Instrumentation (API), Model T500U, USA), CO (Teledyne API, T300U, USA), O_3 (Thermo Electronic Corporation (TEC), Model 49C, USA), and SO_2 (TEC, Model 43C, USA). The meteorological data of temperature, RH, as well as wind direction and speed were monitored by automatic weather station (JZYG, PC-4, China). In addition, VOCs were sampled using stainless-steel canisters and then were delivered to the University of California at Irvine for chemical analysis. Note that the VOCs in the

canister might suffer from a significant decay during the period of approximate one month from sampling in field to chemical analysis in the laboratory (Hsieh et al., 2003). As to the JN site, the trace gas concentrations were taken from the nearest national air quality monitoring station (http://106.37.208.233:20035). The meteorological parameters near the JN site from the website of Weather Underground (https://www.wunderground.com) were also used in this study.

2.3. Chemical analysis of $PM_{2.5}$

The contents of organic carbon (OC) and elemental carbon (EC) in each quartz filter sample were analyzed with a thermal-optical transmittance method and following the NIOSH protocol (Sunset, OCEC analyzer, USA). Further, the concentrations of organic matters (OM) were estimated from the OC contents by multiplying factors of 2.0, 2.1, and 1.8 for the DY site in winter, DY site in summer, and the JN site according to the reported ratios of OM to OC (Turpin and Lim, 2001; Wang et al., 2018a). In addition, inorganic water-soluble ions in $PM_{2.5}$ were analyzed by using ion chromatograph (Dionex Corporation, IC90s, USA) (Luo et al., 2020).

The organics in the particulate were extracted from sample with methanol using a thermostatic orbital shaker for subsequent determination of organic nitrates. The organic extract was enriched by a rotary evaporator and subsequently filtered through a 0.45-μm-porosity PTFE syringe filter. After the methanol in the extract evaporated with nitrogen purging, the residue was immediately reconstituted in methanol with 400 μL of 2 mg L^{-1} tropinone (> 98%, IL, USA) which was used as the internal standard. To determine the recovery during the sample treatment, surrogate standards were dropped onto to blank filters and then processed in the same way with the sample filters.

Sample extracts were analyzed using ultra-performance liquid chromatography (Accela 1250, Thermo Scientific, USA) coupled with electrospray ionization (ESI) source and triple quadrupole tandem mass spectrometry (TSQ Vantage, Thermo Scientific; FWHM = 7500,) and ultra-high performance liquid chromatography (Ultimate 3000, Thermo Scientific) equipped with ESI source and Orbitrap mass spectrometry (Q Exactive Focus, Thermo Scientific; FWHM = 70,000,) in both positive and negative ion modes. Chromatographic column of Atlantis C18 (2.1 × 150 mm, 2.1 μm) was employed for separations at 24 °C. The eluents were methanol (HPLC-grade, Sigma-Aldrich, USA; eluent A) and water with 0.1% formic acid (HPLC-grade, Sigma-Aldrich, USA; eluent B) at 0.2 mL min^{-1}. When the mass spectrometry was operated in positive mode, the gradient elution was as follows: the eluent A was initially set at 30% and the eluent B was 70% for 3 min; eluent A increased to 90% over 10 min and kept for 3 min; then decreased back to 30% A within 0.1 min and kept for 3.9 min. As for the negative mode, the gradient elution started with 3% A and 97% B and kept for 3 min; eluent A increased to 90% over 12 min and kept for 7 min; decreased to 3% within 5 min and then kept for 8 min.

Six kinds of monoterpene and oleic acid-derived particulate organic nitrates (Table S1 and Fig. S1) identified from $PM_{2.5}$ samples in this study. Via monitoring the product ions in MS^2 and MS^3 spectra, monoterpene hydroxyl nitrate (MW = 215, MHN215) and pinene keto nitrate (MW = 229, PKN229) were confirmed from the fragments of *m/z* 46 (loss of NO_2) and m/z 18 (loss of H_2O), which represented the nitrooxy group and hydroxyl group based on the literature report (Perraud et al., 2010). Monoterpene dicarbonyl nitrate (MW = 247, MDCN247) were identified from the losses of m/z 17 (OH), m/z 18 (H_2O), m/z 46 (NO_2), and m/z 49 (OH + H_2O), which agreed with the structure of carbonyl groups, nitrooxy group, and hydroxyl group. Oleic acid keto nitrate (MW = 359, OAKN359) was detected by the losses of m/z 18 (H_2O), m/z 63 (HNO_3), and m/z 92 ($HNO_3 + C_2H_5$), which coincided with the study by Docherty and Ziemann (2006), representing the carbonyl and the nitrooxy groups in OAKN359. Oleic acid hydroxyl nitrate (MW = 361, OAHN361) was identified with the losses of m/z 18 (H_2O), m/z 62 (NO_3), and m/z 106 ($NO_3 + CO_2$) which were consistent with the hydroxyl, the nitrooxy and the carboxyl groups. By monitoring the $[M-H]^-$ ions in negative ion mode, pinene sulfate organic nitrate (MW = 295, PSON295) was recognized based on the fragments of m/z 47 (HNO_2), m/z 63 (HNO_3), m/z 74 ($CO + NO_2$), m/z 96 (SO_4^-), and m/z 80 (SO_3^-) by MS^2 and by MS^3 spectrum, respectively (He et al., 2014). The detailed information has shown in our previous study by Li et al. (2018).

Table 1
Statistics of concentrations of PONs, gaseous pollutants and parameters at sampling sites (average ± standard deviation).

Species/ parameter	Dongying Winter	Dongying Summer	Jinan Autumn
MHN215	88.3 ± 28.1	189 ± 160	51.9 ± 37.6
PKN229	46.6 ± 13.2	96.0 ± 83.0	10.0 ± 10.0
MDCN247	21.6 ± 11.8	17.0 ± 12.3	9.5 ± 7.0
OAKN359	41.6 ± 21.1	103 ± 74.9	34.1 ± 17.4
OAHN361	4.1 ± 1.2	2.0 ± 1.4	0.7 ± 0.8
PSON295	–	8.9 ± 12.4	7.2 ± 7.2
ΣPONs (ng/m^3)	201 ± 47.3	415 ± 207	113 ± 58.6
NO_2 (ppb)	8.2 ± 8.4	4.4 ± 2.5	35.2 ± 15.6
O_3 (ppb)	18.3 ± 10.1	71.2 ± 25.8	22.0 ± 15.5
SO_2 (ppb)	3.7 ± 2.9	2.7 ± 1.6	4.5 ± 1.9
CO (ppm)	0.9 ± 0.6	0.5 ± 0.2	0.8 ± 0.4
OM (μg/m^3)	13 ± 11.4	15 ± 7.7	19 ± 9.4
$PM_{2.5}$ (μg/m^3)	78 ± 52	122 ± 52	70 ± 42
ΣPONs/$PM_{2.5}$ (‰)	3.1 ± 1.1	3.9 ± 2.2	2.3 ± 1.9
ΣPONs/OM (%)	2.6 ± 1.7	2.8 ± 1.1	0.7 ± 0.47
RH (%)	56 ± 11	63 ± 12	47 ± 14
Temperature (°C)	−1.1 ± 1.7	26.4 ± 3.8	12.6 ± 3.3

With consideration of the similar retention time and structures or functional groups, MHN215, PKN229, and MDCN247 were quantified with the surrogate standard of (1*R*, 2*R*, 5*R*)–(+)-2-hydroxy-3-pinanone (GC-grade, TCI, Japan) due to lack of standards. OAKN359 and OAHN361 were quantified with the ricinoleic acid (GC-grade, TCI) for estimation. PSON295 was quantified with the surrogate standard of (−)-10-camphor sulfonic acid (GC-grade, TCI) (He et al., 2014; Worton et al., 2011). Linear fitting curves between the peak area and the standard concentration were established ($r^2 > 0.99$) for quantification. Recoveries of (1R, 2R, 5R)–(+)-2-hydroxy-3-pinanone, ricinoleic acid, and (−)-10-camphor sulfonic acid were 71 ± 9%, 64 ± 4%, and 78 ± 4%, respectively. Based on the uncertainty in the recovery (±12.7%) and the repeatability (±4.1%), the overall uncertainty for the evaluation of PONs was estimated to be 13.3%. Although the use of surrogate standards will enlarge the uncertainty in the absolute concentrations of PONs, these data can still provide significant insights into variation patterns and secondary formation.

3. Results and discussion

3.1. Atmospheric concentration and seasonal variations of PONs

The concentrations of monoterpene and oleic acid-derived PONs at the two sampling sites in the North China Plain were relatively high. Table 1 presents the average concentrations of specific organic nitrates (MHN215, PKN229, MDCN247, OAKN359, OAKN361, and PSON295) as well as gaseous pollutants and meteorological parameters at the DY and JN sampling sites. The total concentration of the six kinds of PONs (ΣPONs) during the observation periods was 113–415 ng m^{-3} on average. Among these monoterpene-derived organic nitrates, MHN215 was the main component with an average concentration of 51.9–189 ng m^{-3}, followed by PKN229 (10.0–96.0 ng m^{-3}), MDCN247 (9.5–21.6 ng m^{-3}), and PSON295 (7.2–8.9 ng m^{-3}). In previous studies, relevant organic nitrate concentrations were in the range of a few to several thousand nanograms per cubic meter (as shown in Table 2). Our observation result was comparable to the reported values in previous observations, though different species and measurement methods were deployed. The monoterpene and oleic acid-derived PONs contributed a relatively small fraction to $PM_{2.5}$, ranging from 2.3‰ to 3.9‰. However, their contribution to OM was notable, with the average mass ratio of

Table 2
Field observation of particulate organic nitrates in previous studies (units: ng m^{-3}).

Location	Site type	Sampling period	Species	Concentration	Surrogate standard	Instrument	Reference
Beijing, China	urban site	May–June 2016	$C_{10}H_{17}NO_7S$	0.6–33.8	synthetic surrogate standard	HPLC–MS	(Wang et al., 2018b)
Beijing, China	urban site	May–June 2016	$C_9H_{15}NO_8S$	0.03–1.5	synthetic surrogate standard	HPLC–MS	(Wang et al., 2018b)
Jinan, China	urban site	April 2016	$C_{10}H_{17}NO_4$, $C_{10}H_{15}NO_5$, $C_{10}H_{17}NO_6$	55.2–112	2-hydroxy-3-pinanone	UHPLC-MS	(Li et al., 2018)
Jinan, China	urban site	April 2016	$C_{18}H_{33}NO_6$, $C_{18}H_{35}NO_6$	23.4–36.8	ricinoleic acid	UHPLC-MS	(Li et al., 2018)
Georgia,US	urban site	August 2015	$C_9H_{15}NSO_8$	0.5	hydroxyacetone sulfate	HILIC-MS/MS	(Hettiyadura et al., 2019)
Guangzhou, China	rural area	September and November 2010	$C_{10}H_{17}NO_7S$	14.4–133	camphor sulfonic acid	LC–MS	(He et al., 2014)
California, US	mountain site	August–October 2007	$C_{10}H_{17}NO_7S$	0.1–4.3	camphor sulfonic acid	UPLC/ MS	(Worton et al., 2011)
Karlsruhe, Germany	rural site	July–August 2016	particulate organic nitrate	>1000	–	CIMS	(Huang et al., 2019)
Cabauw, Netherlands	rural site	May 2008	particulate organic nitrate	≥ 1800	–	AMS	(Reyes-Villegas et al., 2018)

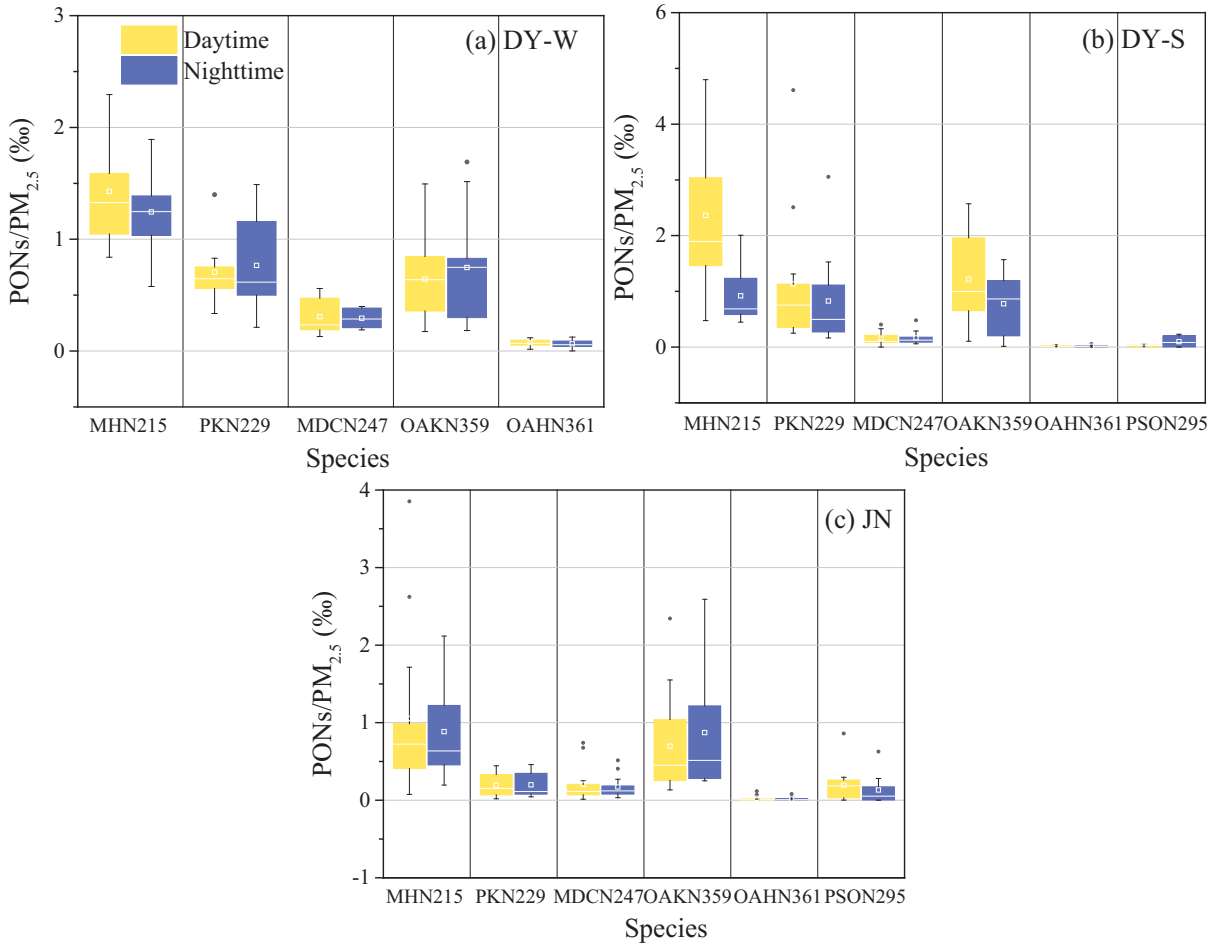

Fig. 2. The differences in PONs/$PM_{2.5}$ ratios during daytime and nighttime at different sampling sites.

ΣPONs to OM varying from 0.7% to 2.8%.

During the observation periods at the DY site, the abundance of PONs exhibited obvious seasonal differences ($p < 0.01$) with the concentration higher in hot season than in cold season. The average abundance of PONs at the DY site in summer was almost twice as high that in winter. This agrees with the observation results in the previous study in Shenzhen in southern China (Yu et al., 2019). The seasonal variations of organic nitrates are usually associated with the changes in precursor emissions, oxidation capacity, air mass transport, and meteorological conditions. Zheng et al. (2010) found that the emissions of BVOCs in the Pearl River Delta region of China exhibited seasonal variations with the peak appearing in summer and the valley in winter. With consideration of the high emission of precursors at the DY site in summer (see Fig. S2) and the intense photochemical activities (71.2 ppb of ozone on average), we attribute the enhanced formation of PONs at the DY site in hot season primarily to the increases in precursor and oxidant concentrations. In addition, the air masses mainly came from the northwest with high altitude in winter. On the contrary, in summer, air masses passed

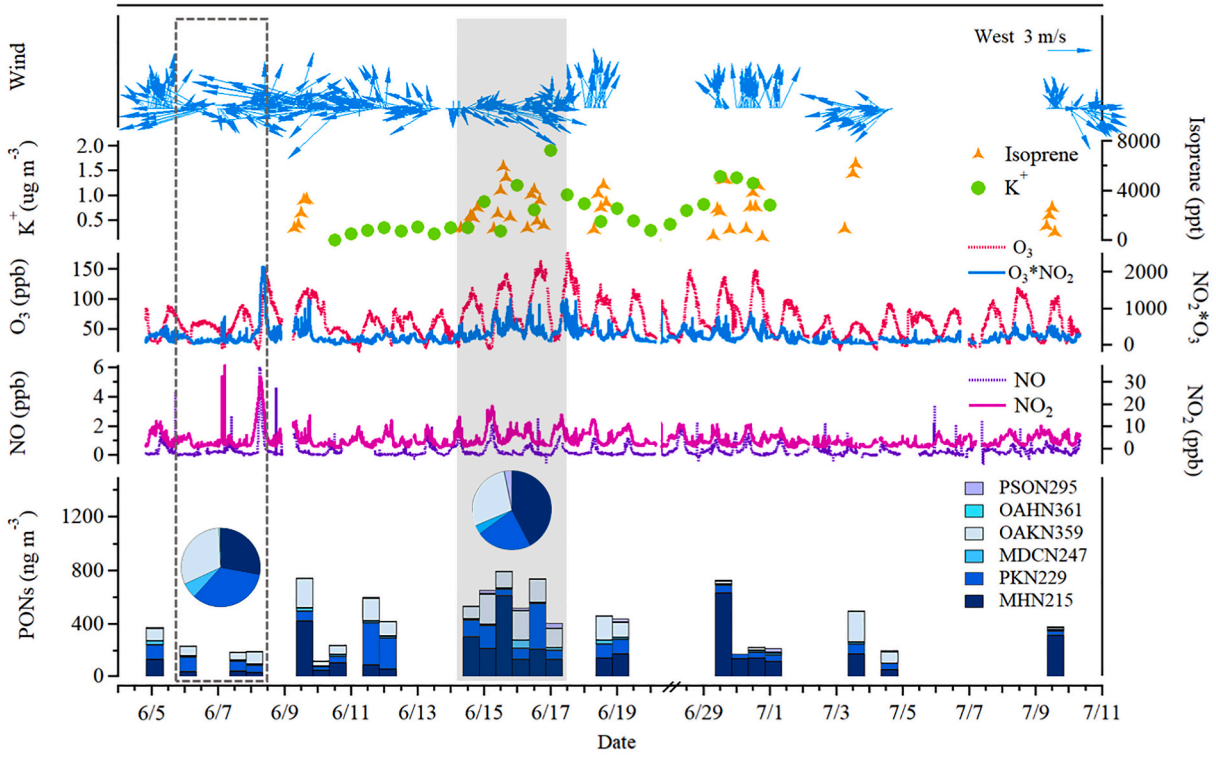

Fig. 3. Time series of wind and concentrations of K^+, isoprene, O_3, NO_2*O_3, NO, NO_2, and PONs at the DY site in summer.

through the southwest and southeast sectors with low altitude, which would transport anthropogenic pollutants and possibly accelerated the formation of PONs.

3.2. Diurnal difference of PONs

Fig. 2 shows the diurnal difference of individual PONs at different sampling sites. Here, the ratio of PONs to $PM_{2.5}$ was presented instead of PON concentration to avoid potential influence from the change in boundary layer height. The daytime fractions of PONs in $PM_{2.5}$ were comparable to those at nighttime ($p > 0.1$) at the DY site in winter and at the JN site. However, at the DY site in summer, MHN215 exhibited an obviously higher proportion at daytime than nighttime ($p < 0.01$). This is consistent with the observation in Japan that the maximum concentration of organic nitrate appeared during the daytime in summer, whereas the diurnal difference is quite small in winter (Sadanaga et al., 2019). Trajectory cluster analysis (shown in Fig. S3) indicates that the trajectory of air masses had no significant diurnal and nocturnal difference during the sampling periods. It means that the air mass transport was not the main reason for diurnal difference. Note that during daytime at the DY site in summer, ozone exhibited very high concentrations and thus enhanced atmospheric oxidation capacity (detailed discussion can be seen in Section 3.3.1). In addition, the emission of precursor BVOCs were larger during daytime because of the high temperature and the intense sunlight (Rinne et al., 2002). Therefore, the relative abundant oxidants and precursors monoterpenes at daytime were likely to produce more monoterpenes-derived organic nitrates. On the contrary, relatively low level of ozone were observed at the DY site in winter and at the JN site when compared to the DY site in summer. Due to the weakening of the photochemical activities during the day in cold seasons, the production rates of organic nitrates from OH-initiated and NO_3-initiated oxidation pathways could be comparable (Sobanski et al., 2017), and thus there was no obvious difference in the fraction of PONs in $PM_{2.5}$ between daytime and nighttime in cold season in this study.

Hydrolysis and photolysis can influence organic nitrate chemistry and atmospheric abundances and have been recently recognized as non-ignorable sinks (Takeuchi and Ng, 2019; Zare et al., 2018). From the observation data in this study, it was difficult to see apparent effects of hydrolysis and photolysis on the concentrations and variations of PONs. With consideration of the moderate humidity at the DY site in summer, hydrolysis was not the main factor of the lower content of PONs at nighttime than daytime. In addition, the concentrations of PONs and their ratios to $PM_{2.5}$ in summer with intensive solar radiation were not lower than those in other seasons. Furthermore, the organic nitrates produced from different precursors have different photochemical aging behaviors, but their photolysis rates are relatively small when compared to their production rates (Luke et al., 1989; Nah et al., 2016). Therefore, photolysis was not regarded as the major factor that governed the diurnal differences of PONs in our study.

3.3. The influences of human activities on PONs

To understand the impacts of human activities on the abundance and formation of PONs, the time series of PONs and their relationships with related indicators for anthropogenic emissions at sampling sites are analyzed in detail here.

3.3.1. Effect of biomass burning on the formation of organic nitrates

Fig. 3 shows the time series of concentrations of PONs, isoprene, potassium (K^+, a tracer of biomass burning), trace gases, as well as the wind direction and speed during the sampling period at the DY site in summer. In the pollution episode from June 14 to 16 (marked by gray shading in Fig. 3), the concentration of PONs was higher than other time periods and MHN215 was the dominant species (42.4%). During this period, the wind mainly came from the southwest and northwest. The concentrations of ozone (up to 160 ppb) and NO_x increased, accompanied by sharply elevated concentrations of isoprene and potassium. By contrast, on June 6 and 7 marked by gray dashed lines, the concentration of PONs was very low with the dominance of the northeastern winds and PKN229 became the major component among these six kinds of

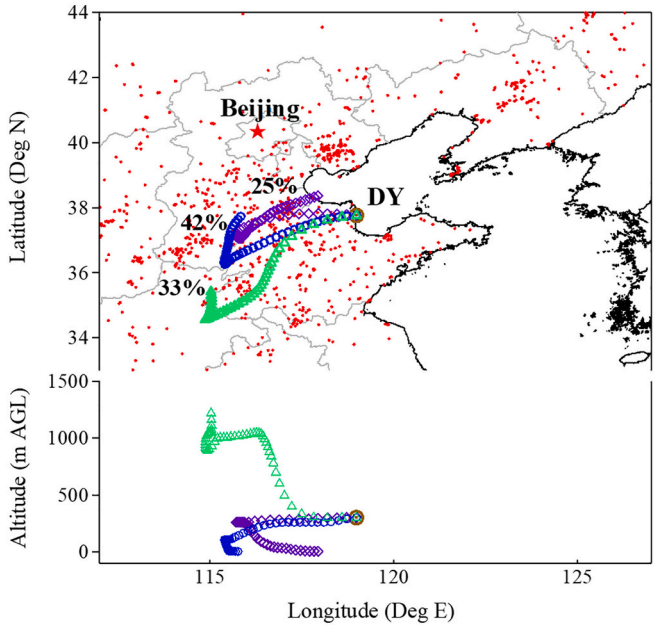

Fig. 4. Distribution of fire spots and the 48-h air mass backward trajectories on 15 June 2017 at the DY site.

PONs. Ozone and NO also appeared at comparatively low concentrations.

In the North China Plain, agricultural crop residues are often burnt in field during the wheat harvest around June (Chen et al., 2017). Further investigation of 48-h air mass backward trajectories with the HYSPLIT model (GDAS data, http://ready.arl.noaa.gov/archives.php) showed that on June 15 the air mass was mainly transported through the west sectors, where widespread and intensive fires had newly emerged (shown in Fig. 4). On the same day, significant enhancement in the concentrations of VOCs were observed. The enrichment of VOCs during the biomass burning period facilitated the photochemical processes and secondary aerosol formation, indicated by the elevated concentrations of ozone and PONs (in particular MHN215). Previous studies have showed that ozone increased by 40–50 ppb and non-fossil carbon fractions of SOA were enhanced as a result of biomass burning (Huang et al., 2014; Xu et al., 2018). Moreover, a large amount of BVOCs can be emitted via biomass burning (Andreae and Merlet, 2001; Xu et al., 2018), as indicated by the nearly doubling of the isoprene concentration on 15 June at the DY site, so it also contributed to the enhanced formation of PONs under the condition of high ozone concentrations.

In addition to the episode during June 14–16, short-term influence from biomass burning was also observed on June 9 and 29. As a result, the concentrations of PONs were high on these two days, with a dominance of MHN215. On June 17 and during the period from June 30 to July 1, the influence from biomass burning weakened and the fine particle concentration decreased, and therefore the concentration of PONs dropped. It was noticed that the composition of PONs on June 16 was similar to that observed during June 6 and 7, i.e., PKN229 became the dominant species, which was possibly because the air mass changed with the wind direction and possibly experienced relatively long aging time.

3.3.2. Effect of coal combustion and SO_2 on the formation of organic nitrates

At the JN and DY sites in winter, field observations reveal that the abundance of PONs was obviously influenced by coal combustion. As shown in Fig. 5, the elevated concentration of PONs usually appeared with concurrent rising SO_2 and CO concentrations. Particularly, at the JN site, the most significant enhancements of PONs and SO_2 were observed from October 21 to 23 (marked by gray shading in Fig. 5). During this episode, MHN215 exhibited the largest proportion (43.4% on average). The ratio of PONs/OM was quite high, indicating the enhanced formation of PONs. However, when the SO_2 concentration was low from October 18 to 30 (marked by the gray dashed lines), the concentration of PONs decreased significantly, though the oxidant level indicated by O_x ($NO_2 + O_3$) were almost equivalent during these two periods. At the same time, the percentage of MHN215 dropped, and OAKN359, mostly came from meat cooking emissions and the subsequent chemical transformation (Rogge et al., 1991) turned to be the dominant component with the average proportion of 44.8%. Further analysis shows that the backward trajectories at the JN site during the period from October 21 to 23 were different from other periods (see Fig. S4). From October 21 to 23, the air mass came from the northeast sector of Jinan where coal-fired industries such as steel plants and thermal power plants are located. Therefore, the relatively high levels of SO_2 are ascribed to the transport of plumes from coal-fired industries in the northeast sector of Jinan City under the influence of northeast winds. Note that the elevated concentration of PONs was also observed during October 20–21, while the SO_2 concentration was very low. During this period, ozone and NO_2 were in high levels, which to a certain degree facilitated the formation of PONs.

As shown in Fig. 6, the correlation between PONs and SO_2 ($r = 0.68$, $p < 0.01$) is stronger than that between PONs and NO_2 ($r = 0.17$, $p < 0.41$) or CO ($r = 0.43$, $p < 0.05$) (see Fig. 6a–c). The different correlation coefficients also indicate that transport was not the controlling factor. Moreover, the ratio of PONs/OM also correlated moderately with SO_2 at the JN site ($r = 0.47$, $p < 0.05$, not shown here). The above results suggest the promotion effect of industrial coal combustion plumes on the PON formation. In previous modeling and observation studies, the important role of coal-fired power plant plumes playing in the formation of organic nitrates has also been recognized (Fibiger et al., 2018; Fry et al., 2018).

The similar enhancement of PONs caused by coal combustion was also observed at the DY site in winter. The concentration of PONs was up to 369 ng m^{-3} at the daytime on January 19, accompanied by the maximum concentrations of SO_2 and $PM_{2.5}$ (13.2 ppb and 229 μg m^{-3}, respectively) during the observation period. The significant increases in SO_2 and $PM_{2.5}$ concentrations were ascribed to the coal-fired plume from the rural areas nearby for heating demand. The 4-nitrophenol (4NP) and 5-nitrosalicylic acid (5NSA), which are abundant in fresh coal combustion flue gas (Lu et al., 2019), exhibited similar trends with SO_2 and PONs, indicating the potential effect of residential coal combustion on the concentrations of PONs. Further correlation analysis shows that PONs and SO_2 at the DY site in winter exhibited a strong positive linear relationship ($r = 0.88$, $p < 0.01$; as shown in Fig. 6d). PONs was also correlated with CO ($r = 0.61$, $p < 0.01$; see Fig. 6e), which indicates that the transport had an effect on the concentration of PONs at DY site in winter.

Overall, the concurrent appearance of elevated concentrations (and fractions) of PONs and SO_2 at the JN site and at the DY site in winter was suggestive of the potential influence of industrial and residential coal combustion on the abundances of PONs. On the one hand, the direct fast reactions between SO_2 and monoterpene-derived Criegee intermediates could facilitate the production of intermediate products of organic nitrates, and thus promoted the formation of PONs (Zhang et al., 2020) On the other hand, the vapor plumes and fuel gas emitted from coal-fired power plants were very acidic (Hlawiczka et al., 2016). Sulfuric acid, an important nucleating agent, was conducive to SOA production including PONs via providing seed aerosols and facilitating the acid-catalyzed reactions (Chu et al., 2016; Han et al., 2016). To date, the roles of SO_2 and acidic sulfate aerosols in the formation of organic nitrates has not been fully understood. More in-depth investigations are needed to better understand the formation and oxidation mechanism.

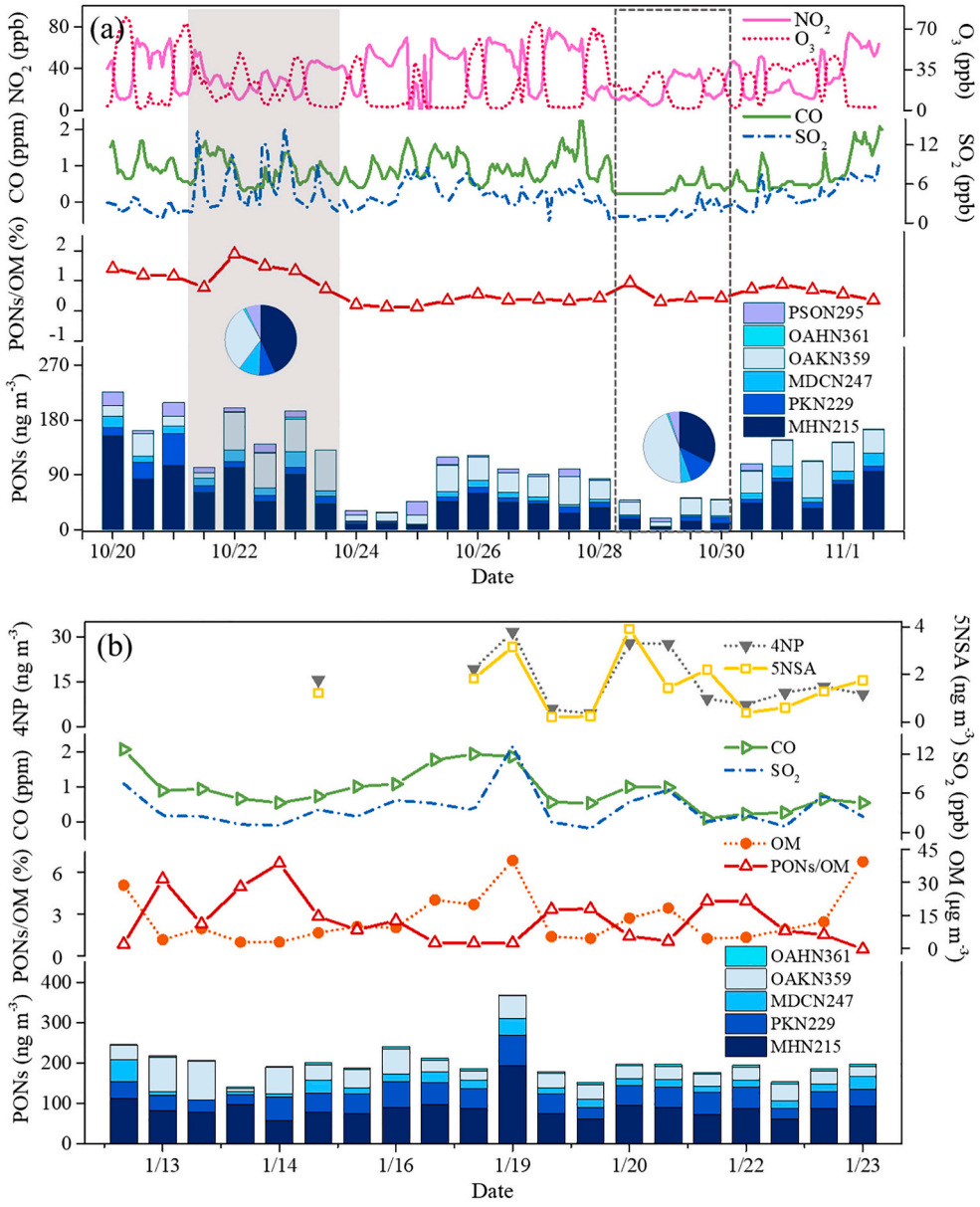

Fig. 5. Time series of PONs, PONs/OM, and relevant gaseous and particulate pollutants (a) at JN site and (b) at DY site in winter.

4. Conclusion

Six kinds of monoterpene and oleic acid-derived PONs at rural and urban areas in the North China Plain were determined and the spatial and temporal variations as well as the influence of human activities on these species were investigated. The concentration of PONs was obviously higher in summer than that in winter at the rural DY site. In summer, the day time concentration of MHN215 at the DY site was higher than that at night, while the diurnal difference was small in other seasons. Concurrent variations of PONs with anthropogenic pollutants and correlation analyses indicated human activities have a significant impact on PON abundance in the North China Plain. During the biomass burning period, the formation of ozone was promoted and the abundance of BVOCs was enhanced, thus facilitating the photochemical reactions for PONs. In addition, the observed increase in the concentration of PONs was consistent with the SO_2 variation pattern in coal combustion plumes, indicating the promotion effects of SO_2 and acidic sulfate aerosols on PON formation. This study highlights that a coupled anthropogenic–biogenic source is regionally non-neglectable for the atmospheric abundance of PONs and more in-depth studies are needed to better understand the formation pathways.

Declaration of Competing Interest

The authors declare that they have no known competing financial interests or personal relationships that could have appeared to influence the work reported in this paper.

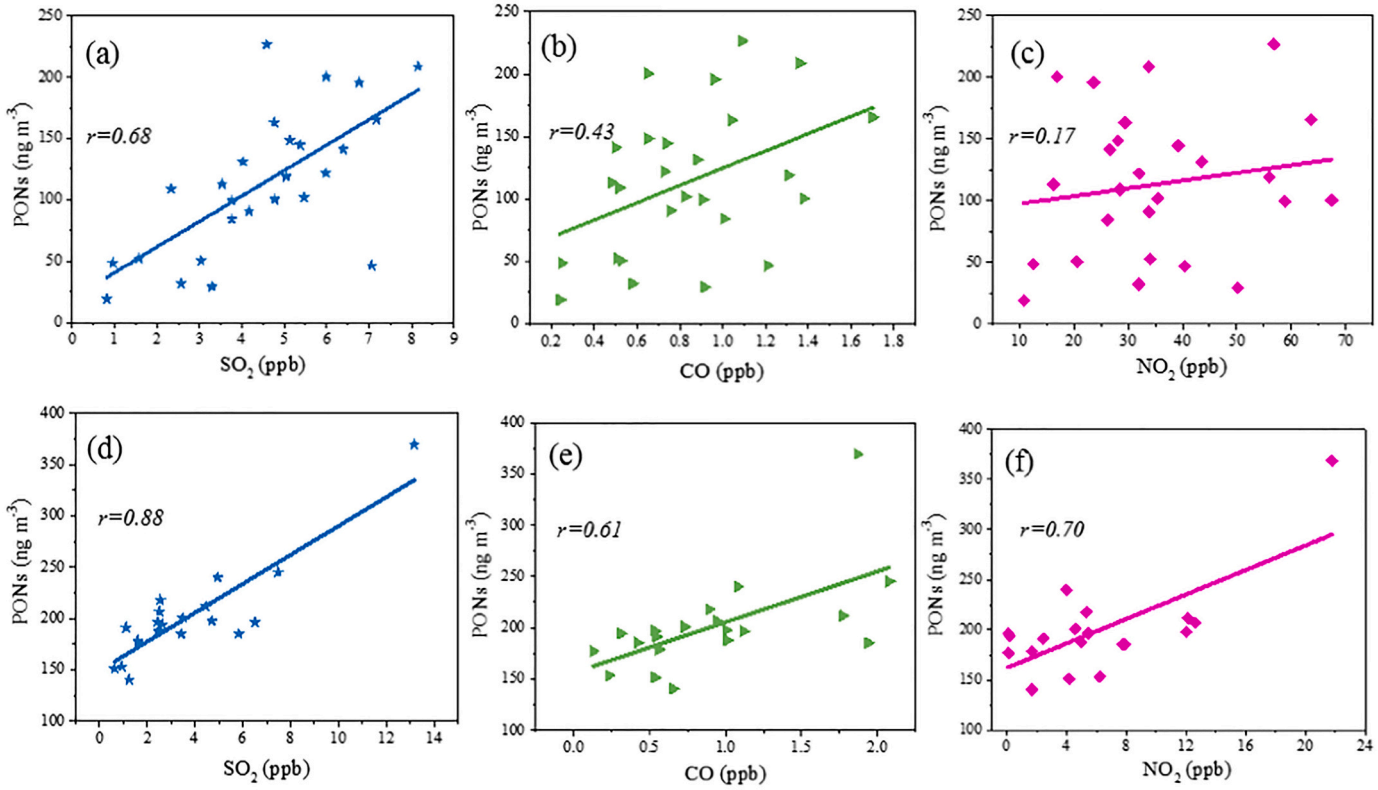

Fig. 6. Correlation between PONs and SO_2, CO, and NO_2 at the JN site and DY site in winter.

Acknowledgements

This work was supported by National Natural Science Foundation of China (nos. 41775118, 91644214, 91544213, 41675118), the Youth Innovation Program of Universities in Shandong Province (2019KJD007), and the State Key Laboratory of Organic Geochemistry, GIGCAS (Grant No. SKLOG-201616) and received financial support from Shandong University (grant no. 2020QNQT012). The authors would like to thank the website of China National Environmental Monitoring Centre (http://106.37.208.233:20035) and Weather Underground (https://www.wunderground.com) for providing the trace gas and meteorological data.

Appendix A. Supplementary data

Supporting information to this article can be found online at https://doi.org/10.1016/j.atmosres.2021.105585.

References

Andreae, M.O., Merlet, P., 2001. Emission of trace gases and aerosols from biomass burning. Glob. Biogeochem. CY 15, 955–966.

Brown, S.S., Dubé, W.P., Karamchandani, P., Yarwood, G., Peischl, J., Ryerson, T.B., et al., 2012. Effects of NO_x control and plume mixing on nighttime chemical processing of plumes from coal-fired power plants. J. Geophys. Res. 117.

Chen, J., Li, C., Ristovski, Z., Milic, A., Gu, Y., Islam, M.S., et al., 2017. A review of biomass burning: emissions and impacts on air quality, health and climate in China. Sci. Total Environ. 579, 1000–1034.

Chu, B., Zhang, X., Liu, Y., He, H., Sun, Y., Jiang, J., et al., 2016. Synergetic formation of secondary inorganic and organic aerosol: effect of SO_2 and NH_3 on particle formation and growth. Atmos. Chem. Phys. 16, 14219–14230.

Day, D.A., Liu, S., Russell, L.M., Ziemann, P.J., 2010. Organonitrate group concentrations in submicron particles with high nitrate and organic fractions in coastal southern California. Atmos. Environ. 44, 1970–1979.

de Oliveira Alves, N., de Souza Hacon, S., de Oliveira, Galvão M.F., Simões, Peixotoc M., Artaxo, P., de Castro Vasconcellos, P., et al., 2014. Genetic damage of organic matter in the Brazilian Amazon: a comparative study between intense and moderate biomass burning. Environ. Res. 130, 51–58.

Docherty, K.S., Ziemann, P.J., 2006. Reaction of oleic acid particles with NO_3 radicals: products, mechanism, and implications for radical-initiated organic aerosol oxidation. J. Phys. Chem. A 110, 3567–3577.

Ehn, M., Thornton, J.A., Kleist, E., Sipilä, M., Junninen, H., Pullinen, I., et al., 2014. A large source of low-volatility secondary organic aerosol. Nature 506, 476–479.

Fibiger, D.L., McDuffie, E.E., Dubé, W.P., Aikin, K.C., Lopez-Hilfiker, F.D., Lee, B.H., et al., 2018. Wintertime overnight NO_x removal in a southeastern United States coal-fired power plant plume: a model for understanding winter NO_x processing and its implications. J. Geophys. Res. 123, 1412–1425.

Fry, J.L., Brown, S.S., Middlebrook, A.M., Edwards, P.M., Campuzano-Jost, P., Day, D.A., et al., 2018. Secondary organic aerosol (SOA) yields from NO_3 radical + isoprene based on nighttime aircraft power plant plume transects. Atmos. Chem. Phys. 18, 11663–11682.

Guo, S., Hu, M., Zamora, M.L., Peng, J., Shang, D., Zheng, J., et al., 2014. Elucidating severe urban haze formation in China. Proc. Natl. Acad. Sci. 111, 17373–17378.

Hallquist, M., Wenger, J.C., Baltensperger, U., Rudich, Y., Simpson, D., Claeys, M., et al., 2009. The formation, properties and impact of secondary organic aerosol: current and emerging issues. Atmos. Chem. Phys. 9, 5155–5236.

Han, Y., Stroud, C.A., Liggio, J., Li, S.M., 2016. The effect of particle acidity on secondary organic aerosol formation from α-pinene photooxidation under atmospherically relevant conditions. Atmos. Chem. Phys. 16, 13929–13944.

He, Q.F., Ding, X., Wang, X.M., Yu, J.Z., Fu, X.X., Liu, T.Y., et al., 2014. Organosulfates from pinene and isoprene over the Pearl River Delta, South China: seasonal variation and implication in formation mechanisms. Environ. Sci. Technol. 48, 9236–9245.

Hettiyadura, A.P.S., Al-Naiema, I.M., Hughes, D.D., Fang, T., Stone, E.A., 2019. Organosulfates in Atlanta, Georgia: anthropogenic influences on biogenic secondary organic aerosol formation. Atmos. Chem. Phys. 19, 3191–3206.

Hlawiczka, S., Korszun, K., Fudala, J., 2016. Acidity of vapor plume from cooling tower mixed with flue gases emitted from coal-fired power plant. Sci. Total Environ. 554-555, 253–258.

Horowitz, L.W., Fiore, A.M., Milly, G.P., Cohen, R.C., Perring, A., Wooldridge, P.J., et al., 2007. Observational constraints on the chemistry of isoprene nitrates over the eastern United States. J. Geophys. Res. A 112.

Hsieh, C.C., Horng, S.H., Liao, P.N., 2003. Stability of trace-level volatile organic compounds stored in canisters and tedlar bags. Aerosol Air Qual. Res. 3, 17–28.

Huang, R.J., Zhang, Y., Bozzetti, C., Ho, K.F., Cao, J.J., Han, Y., et al., 2014. High secondary aerosol contribution to particulate pollution during haze events in China. Nature 514, 218–222.

Huang, W., Saathoff, H., Shen, X., Ramisetty, R., Leisner, T., Mohr, C., 2019. Chemical characterization of highly functionalized organonitrates contributing to night-time organic aerosol mass loadings and particle growth. Environ. Sci. Technol. 53, 1165–1174.

Kiendler-Scharr, A., Mensah, A.A., Friese, E., Topping, D., Nemitz, E., Prevot, A.S.H., et al., 2016. Ubiquity of organic nitrates from nighttime chemistry in the European submicron aerosol. Geophys. Res. Lett. 43, 7735–7744.

Li, R., Wang, X.F., Gu, R.R., Lu, C.Y., Zhu, F.P., Xue, L.K., et al., 2018. Identification and semi-quantification of biogenic organic nitrates in ambient particulate matters by UHPLC/ESI-MS. Atmos. Environ. 176, 140–147.
Liu, X., Bai, X., Tian, H., Wang, K., Hua, S., Liu, H., et al., 2020. Fine particulate matter pollution in North China: seasonal-spatial variations, source apportionment, sector and regional transport contributions. Environ. Res. 184.
Lu, C., Wang, X., Li, R., Gu, R., Zhang, Y., Li, W., et al., 2019. Emissions of fine particulate nitrated phenols from residential coal combustion in China. Atmos. Environ. 203, 10–17.
Luke, W.T., Dickerson, R.R., Nunnermacker, L.J., 1989. Direct measurements of the photolysis rate coefficients and Henry's law constants of several alkyl nitrates. J. Geophys. Res. 94, 14905–14921.
Luo, Y., Zhou, X., Zhang, J., Xue, L., Chen, T., Zheng, P., et al., 2020. Characteristics of airborne water-soluble organic carbon (WSOC) at a background site of the North China Plain. Atmos. Res. 231, 104668.
Nah, T., Sanchez, J., Boyd, C.M., Ng, N.L., 2016. Photochemical aging of alpha-pinene and beta-pinene secondary organic aerosol formed from nitrate radical oxidation. Environ. Sci. Technol. 50, 222–231.
Ng, N.L., Brown, S.S., Archibald, A.T., Atlas, E., Cohen, R.C., Crowley, J.N., et al., 2017. Nitrate radicals and biogenic volatile organic compounds: oxidation, mechanisms, and organic aerosol. Atmos. Chem. Phys. 17, 2103–2162.
Novakov, T., Penner, J.E., 1993. The addition of a polar nitrate group to condensed phase organics in the aerosol may change the hygroscopicity of the aerosol and may thus alter the CCN activity of the particle. Nature 365, 823.
Perraud, V., Bruns, E.A., Ezell, M.J., Johnson, S.N., Greaves, J., Finlayson-Pitts, B.J., 2010. Identification of organic nitrates in the NO_3 radical initiated oxidation of α-pinene by atmospheric pressure chemical ionization mass spectrometry. Environ. Sci. Technol. 44, 5887–5893.
Pye, H.O.T., Luecken, D.J., Xu, L., Boyd, C.M., Ng, N.L., Baker, K.R., et al., 2015. Modeling the current and future roles of particulate organic nitrates in the southeastern United States. Environ. Sci. Technol. 49, 14195–14203.
Reyes-Villegas, E., Priestley, M., Ting, Y.C., Haslett, S., Bannan, T., Le Breton, M., et al., 2018. Simultaneous aerosol mass spectrometry and chemical ionisation mass spectrometry measurements during a biomass burning event in the UK: insights into nitrate chemistry. Atmos. Chem. Phys. 18, 4093–4111.
Rinne, H.J.I., Guenther, A.B., Greenberg, J.P., Harley, P.C., 2002. Isoprene and monoterpene fluxes measured above Amazonian rainforest and their dependence on light and temperature. Atmos. Environ. 36, 2421–2426.
Rollins, A.W., Browne, E.C., Min, K.E., Pusede, S.E., Wooldridge, P.J., Gentner, D.R., et al., 2012. Evidence for NO_x control over nighttime SOA formation. Science 337, 1210–1212.
Sadanaga, Y., Ishiyama, A., Takaji, R., Matsuki, A., Kato, S., Sato, K., et al., 2019. Behavior of total peroxy and total organic nitrate concentrations at Suzu on the Noto Peninsula, Japan: long-range transport and local photochemical production. Atmos. Environ. 196, 20–26.
Shi, X., Qiu, X., Cheng, Z., Chen, Q., Rudich, Y., Zhu, T., 2020. Isomeric identification of particle-phase organic nitrates through gas chromatography and time-of-flight mass spectrometry coupled with an electron capture negative ionization source. Environ. Sci. Technol. 54, 707–713.
Sobanski, N., Thieser, J., Schuladen, J., Sauvage, C., Song, W., Williams, J., et al., 2017. Day and night-time formation of organic nitrates at a forested mountain site in south-west Germany. Atmos. Chem. Phys. 17, 4115–4130.
Takeuchi, M., Ng, N.L., 2019. Chemical composition and hydrolysis of organic nitrate aerosol formed from hydroxyl and nitrate radical oxidation of α-pinene and β-pinene. Atmos. Chem. Phys. 12749–12766.
Turpin, B.J., Lim, H.J., 2001. Species contributions to $PM_{2.5}$ mass concentrations: revisiting common assumptions for estimating organic mass. Aerosol Sci. Technol. 35, 602–610.
Wang, X., Chen, J., Sun, J., Li, W., Yang, L., Wen, L., et al., 2014. Severe haze episodes and seriously polluted fog water in Ji'nan, China. Sci. Total Environ. 493, 133–137.
Wang, L., Wang, X., Gu, R., Wang, H., Yao, L., Wen, L., et al., 2018a. Observations of fine particulate nitrated phenols in four sites in northern China: concentrations, source apportionment, and secondary formation. Atmos. Chem. Phys. 18, 4349–4359.
Wang, Y.J., Hu, M., Guo, S., Wang, Y.C., Zheng, J., Yang, Y.D., et al., 2018b. The secondary formation of organosulfates under interactions between biogenic emissions and anthropogenic pollutants in summer in Beijing. Atmos. Chem. Phys. 18, 10693–10713.
Wen, L., Xue, L., Wang, X., Xu, C., Chen, T., Yang, L., et al., 2018. Summertime fine particulate nitrate pollution in the North China Plain: increasing trends, formation mechanisms and implications for control policy. Atmos. Chem. Phys. 18, 11261–11275.
Worton, D.R., Goldstein, A.H., Farmer, D.K., Docherty, K.S., Jimenez, J.L., Gilman, J.B., et al., 2011. Origins and composition of fine atmospheric carbonaceous aerosol in the Sierra Nevada Mountains, California. Atmos. Chem. Phys. 11, 10219–10241.
Xu, L., Suresh, S., Guo, H., Weber, R.J., Ng, N.L., 2015. Aerosol characterization over the southeastern United States using high-resolution aerosol mass spectrometry: spatial and seasonal variation of aerosol composition and sources with a focus on organic nitrates. Atmos. Chem. Phys. 15, 7307–7336.
Xu, Z., Huang, X., Nie, W., Shen, Y., Zheng, L., Xie, Y., et al., 2018. Impact of biomass burning and vertical mixing of residual-layer aged plumes on ozone in the Yangtze River Delta, China: a tethered-balloon measurement and modeling study of a multiday ozone episode. J. Geophys. Res. 123, 11,786–11,803.
Xu, L., Tsona, N.T., You, B., Zhang, Y., Wang, S., Yang, Z., et al., 2020. NO_x enhances secondary organic aerosol formation from nighttime γ-terpinene ozonolysis. Atmos. Environ. 225, 117375.
Yu, L., Wang, G., Zhang, R., Zhang, L., Song, Y.U., Wu, B., et al., 2013. Characterization and source apportionment of $PM_{2.5}$ in an urban environment in Beijing. Aerosol Air Qual. Res. 13, 574–583.
Yu, K., Zhu, Q., Du, K., Huang, X.-F., 2019. Characterization of nighttime formation of particulate organic nitrates based on high-resolution aerosol mass spectrometry in an urban atmosphere in China. Atmos. Chem. Phys. 19, 5235–5249.
Zare, A., Romer, P.S., Nguyen, T., Keutsch, F.N., Skog, K., Cohen, R.C., 2018. A comprehensive organic nitrate chemistry: insights into the lifetime of atmospheric organic nitrates. Atmos. Chem. Phys. 18, 15419–15436.
Zhang, J.K., Cheng, M.T., Ji, D.S., Liu, Z.R., Hu, B., Sun, Y., et al., 2016. Characterization of submicron particles during biomass burning and coal combustion periods in Beijing, China. Sci. Total Environ. 562, 812–821.
Zhang, Y., Sun, J., Zheng, P., Chen, T., Liu, Y., Han, G., et al., 2019. Observations of C1–C5 alkyl nitrates in the Yellow River Delta, northern China: effects of biomass burning and oil field emissions. Sci. Total Environ. 656, 129–139.
Zhang, J., Wang, X.F., Zhang, Y.N., Gu, R.R., Xia, M., Li, H., et al., 2020. Pollution characteristics and formation of particulate organic nitrates in winter in Beijing City. Geochimica 49, 252–261.
Zhao, D., Schmitt, S.H., Wang, M., Acir, I.-H., Tillmann, R., Tan, Z., et al., 2018. Effects of NO_x and SO_2 on the secondary organic aerosol formation from photooxidation of α-pinene and limonene. Atmos. Chem. Phys. 18, 1611–1628.
Zheng, J., Zheng, Z., Yu, Y., Zhong, L., 2010. Temporal, spatial characteristics and uncertainty of biogenic VOC emissions in the Pearl River Delta region, China. Atmos. Environ. 44, 1960–1969.
Ziemann, P.J., Atkinson, R., 2012. Kinetics, products, and mechanisms of secondary organic aerosol formation. Chem. Soc. Rev. 41, 6582–6605.
Zong, Z., Tan, Y., Wang, X., Tian, C., Fang, Y., Chen, Y., et al., 2018. Assessment and quantification of NO_x sources at a regional background site in North China: comparative results from a Bayesian isotopic mixing model and a positive matrix factorization model. Environ. Pollut. 242, 1379–1386.